Research Article

OPENPUB Journal of Cancer Research & Reviews

OPENPUB GLOBAL PUBLISHERS

Received: 01-04-2025 **Accepted:** 08-04-2025 **Published:** 15-04-2025

Volume 1 | Issue 1

Development and Assessment of A Unique Disulfidptosis-Associated Lncrna Profile for Immune Microenvironment Prediction and Personalized Therapy in Gastric Adenocarcinoma

Jiyue Zhu[1,2], Xiang Zhu[1,2], Tingting Su[1], Huiqing Zhou[3], Shouhua Wang[1,2*], Weibin Shi[1,2*]

[1]Department of General Surgery, Xinhua Hospital, Shanghai Jiao Tong University School of Medicine, Shanghai, 200092, China.

[2]Shanghai Key Laboratory of Biliary Tract Disease Research, Shanghai, 200092, China.

[3]Department of Gastroenterology, Xinhua Hospital, Shanghai Jiao Tong University School of Medicine, Shanghai, China.

[*]**Corresponding author:** Shi Weibin, Department of General Surgery, Xinhua Hospital, Shanghai Jiao Tong University School of Medicine, Shanghai, 200092, China.

Citation: Zhu J, Zhu X, Su T, Zhou H, Wang S, et al. (2025). Development and Assessment of A Unique Disulfidptosis-Associated Lncrna Profile for Immune Microenvironment Prediction and Personalized Therapy in Gastric Adenocarcinoma. OPENPUB J of Cancer Res & Rev. 1(2): 01-12.

Abstract

Background: Long non-coding RNAs (lncRNAs) are crucial factors affecting the occur-rence, progression and prognosis of gastric cancer. Accumulation of disulfide bonds to excessive levels in cells expressing high SLC7A11 triggers disulfidptosis, which functions as a regulated form of cellular death. Research have demonstrated that upregulated SLC7A11 is common in human cancers, but the effect of disulfidptosis on gastric cancer remains unclear. Identifying long non-coding RNAs associated with disulfidptosis (drlncRNAs) and establishing a prognostic risk profile holds considerable importance for advancing gastric cancer research and treatment. Methods: Clinical records and transcriptomic datasets from individuals with gastric cancer were acquired from The Cancer Genome Atlas (TCGA) repository. A 3 drlncRNAs risk model was built by three common regression analysis methods. Then we used ROC curves, independent prognostic analysis and additional statistical approaches to assess the precision of the model. This investi-gation additionally encompassed GO and KEGG analysis, immune cell infiltration evaluation, and pharmacological sensitivity predictions. To further investigate immunotherapy response dis-parities between patient cohorts with elevated and reduced risk scores, analyses of TMB, MSI, and TIDE were implemented. Results: We constructed a unique model composed of 3 drlncRNAs (AC107021.2, AC016394.2 and AC129507.1).

Independent prognostic capability for gastric carci-noma patients was validated through both single-variable and multivariable Cox regression analyses. GO and KEGG pathway assessments revealed predominant enrichment within the el-evated-risk cohort, particularly in pathways involving sulfur compound interactions, traditional WNT signaling mechanisms, cellular-substrate adhesion junctions, and cAMP signaling cascades, among others. TME evaluation demonstrated elevated ImmuneScores, StromalScores, and ES-TIMATEScores within the high-risk patient population. Concurrently, this elevated-risk cohort exhibited enhanced immune cell infiltration patterns, whereas the reduced-risk group displayed superior expression of ICPs. Additional investigations revealed that patients categorized in the reduced-risk classification possessed greater tumor mutational burden, increased microsatellite instability-high proportions, and diminished Tumor Immune Dysfunction and Exclusion scores compared to their high-risk counterparts. Pharmacological sensitivity assessments confirmed superior efficacy of several therapeutic agents, including gemcitabine and veliparib (ABT.888), in patients with lower risk classifications. Conclusively, our established risk stratification system demonstrates independent prognostic predictive capacity while offering personalized clinical intervention guidance for individuals diagnosed with gastric carcinoma.

Keywords: Gastric cancer, disulfidptosis, lncRNA, TCGA, prognostic model, immune status.

1. Introduction

Globally, gastric carcinoma ranks among the most prevalent malignancies, with an-nual worldwide incidence approaching 1 million new diagnoses and mortality exceeding 720,000 individuals annually[1]. Epidemiological data from 2020 documented 1.1 million newly identified cases and approximately 770,000 fatalities attributed to this gastrointes-tinal malignancy worldwide. Projections suggest a substantial escalation in these figures, with epidemiological forecasts anticipating approximately 1.8 million additional diagno-ses and 1.3 million gastric cancer-related mortalities by 2040.[2]. Early gastric cancer typ-ically presents with subtle and nonspecific symptoms, resulting in more than 60% of pa-tients being diagnosed after metastasis[3]. This late diagnosis contributes to poor progno-sis, with only 5% of patients with metastatic GC surviving beyond five years[4,5].

Fortunately, therapeutic advances in immunological interventions, particularly im-mune checkpoint blockade agents (ICBs), have offered promising approaches for manag-ing progressive and relapsed gastric malignancies[6]. Nevertheless, a considerable per-centage (40-60%) of individuals receiving immune checkpoint-targeted therapies exhibit therapeutic resistance[7]. Consequently, identifying dependable prognostic indicators to anticipate survival outcomes in gastric adenocarcinoma (STAD) patients, recognizing treatment-responsive populations and effective pharmaceutical agents holds paramount importance for ultimately enhancing longevity among individuals with gastric carcino-ma.

Disulfidptosis is a kind of original regulated cell death that is different from ferropto-sis and cuproptosis. Initial characterization by Liu and colleagues established disul-fidptosis as a distinct cellular death mechanism triggered by disulfide bond overaccumu-lation within cells expressing elevated levels of SLC7A11. Here we focus on drlncRNAs related to 24 DRGs (disulfidptosis-related genes) mentioned in the literature including GYS1, NDUFS1, OXSM, LRPPRC, NDUFA11, NUBPL, NCKAP1, RPN1, SLC3A2, SLC7A11, INF2, CD2AP, ACTN4, PDLIM1, IQGAP1, DSTN, CAPZB, ACTB, MYL6, MYH9, MYH10, TLN1, FLNA, FLNB. Among these 24 DRGs, the last 14 are genes that encode actin-related proteins and upregulate following the glucose starvation[8]. Given that up-regulated SLC7A11 is common in human cancers, the discovery of disulfidptosis expands the framework of programmed cell death and may lead to new treatment and therapeutic targets for multiple cancers [9-11].

Expanding scientific literature demonstrates that long non-coding RNAs functioning as oncogenic elements can enhance proliferative capacity, invasive potential, and meta-static dissemination in gastric carcinoma cells, while simultaneously serving as prospec-tive molecular indicators for survival prognostication and personalized therapeutic deci-sion-making in gastric adenocarcinoma patients.[12-15]. However, disulfidptosis-related lncRNA in STAD have barely been reported so far.

This investigation endeavors to establish an innovative lncRNA profile associated with disulfidptosis for prognostic assessment and immune microenvironment character-ization in gastric adenocarcinoma. We anticipate that our findings will contribute signifi-cant insights toward identifying efficacious therapeutic compounds and selecting patients most likely to benefit from immunological interventions.

2. Materials and methods

2.1. Date source

The methodological framework of this investigation is illustrated in Figure-1. Tran-scriptomic datasets comprising 448 gastric adenocarcinoma cases (412 neoplastic speci-mens and 36 non-neoplastic tissues) along with clinical information from 443 patients were acquired from The Cancer Genome Atlas (TCGA) repository (https://tcga-data.nci.nih.gov/tcga/). For differentiation between messenger RNAs and long non-coding RNAs, we utilized Strawberry Perl computational platform (version 5.30.0-64bit) obtained from https://strawberryperl.com/. 24 DRGs were collected from the literature by Liu et al. mentioned before and Pearson correlation analysis was then per-formed to filter out drlncRNAs. In order to minimize errors, patients with missing surviv-al information were excluded and 407 STAD patients remained eventually. Simple nucle-otide variation (SNV) profiles from 434 gastric adenocarcinoma subjects were additionally extracted from The Cancer Genome Atlas repository and subsequently employed for tu-mor mutational burden (TMB) quantification. The data of STAD microsatellite status were obtained from TCIA website (https://www.tcia.at/). Tumor Immune Dysfunction and Exclusion (TIDE) metrics were procured from the Harvard Dana-Farber Cancer Institute online platform (http://tide.dfci.harvard.edu).

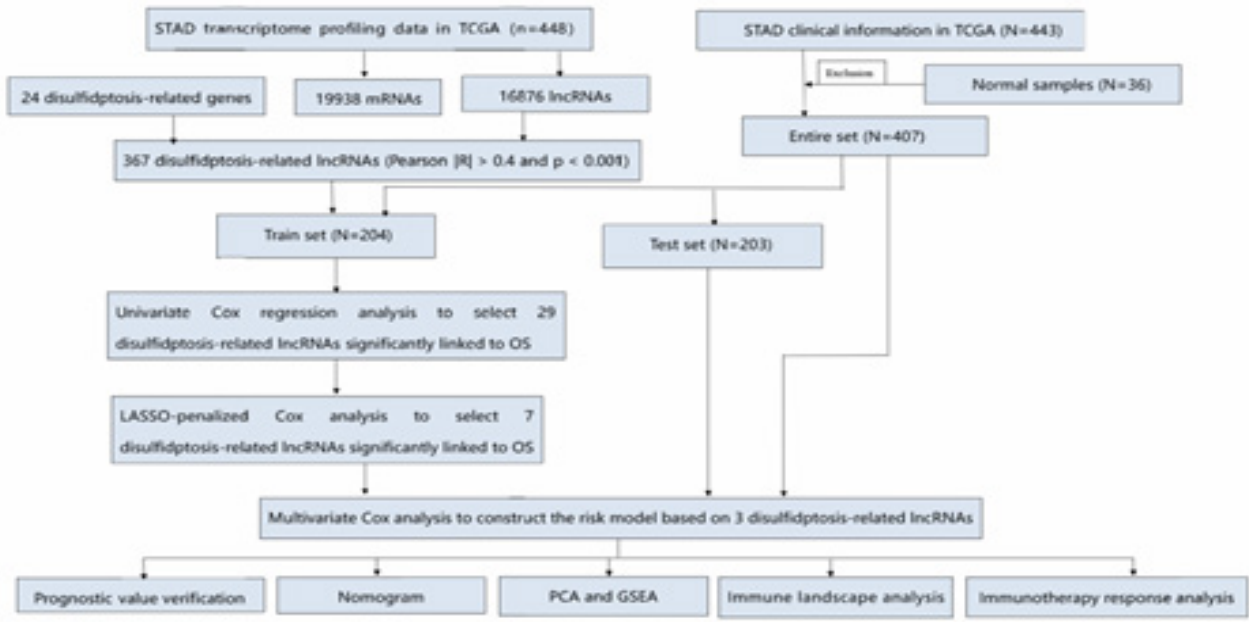

Figure 1. The methodological framework of the present study.

2.2. The development and verification of the arlncRNAs signature

The comprehensive cohort encompassing 407 gastric adenocarcinoma cases under-went random allocation into training and validation datasets at an equal 1:1 distribution ratio. Then, statistical analysis was implemented to substantiate the classification robust-ness. We first developed the drlncRNA prognostic model in the train set. Application of univariate Cox proportional hazards regression identified 29 disulfidptosis-associated long non-coding RNAs exhibiting substantial association with overall survival (OS) ($p<0.05$). To mitigate potential overfitting issues, we subsequently implemented least ab-solute shrinkage and selection operator (LASSO)-penalized Cox methodology with 10-fold cross-validation under identical significance thresholds ($p<0.05$), yielding 7 candidate transcripts. Multivariable Cox regression analysis further refined this selection, culminat-ing in a prognostic algorithm incorporating 3 disulfidptosis-related long non-coding RNAs. Model performance underwent verification utilizing both the validation cohort and the aggregate patient population. Risk stratification scores were derived according to the following mathematical expression:

Risk score= lncRNA1exp × coef1 + lncRNA2exp × coef2 +… + lncRNAnexp × coefn.

lncRNAnexp: expression of lncRNAn

coefn: risk coefficient of lncRNAn based on the model

Based on the median computed risk value as the threshold criterion, all gastric ade-nocarcinoma subjects were stratified into elevated and reduced disulfidptosis score cate-gories. The prognostic algorithm's precision was evaluated through independent survival analyses to determine whether this disulfidptosis-associated long non-coding RNA pro-file could predict clinical outcomes in gastric carcinoma patients autonomously from de-mographic variables (age and gender) and tumor characteristics (histological grade and pathological stage). Subsequently, we used R packages "survival", "survminer" and "tim-eROC" to plot ROC curves of the train set, test set, entire set and different clinicopatholog-ical characteristics respectively, and corresponding AUC (area under curve) value were also calculated. To further corroborate our prognostic algorithm's efficacy, survival anal-yses employing Kaplan-Meier methodology were conducted across various clinicopatho-logical parameters including patient age, histological differentiation, disease progression stage, primary tumor dimensions (T classification), regional lymphatic involvement (N classification), and remote metastatic status (M classification).

2.3. Independent prognostic analysis and ROC curve plotting

Independent prognostic analysis was utilized to corroborate that our model can pre-dict the outcomes of patients independent of age, gender, stage and grade. The predictive precision of the prognostic model was assessed through ROC curves and AUC (area un-der curve) values. (R packages "limma",

"scatterplot3d", "survival", "survminer" and "timeROC" were used in this progress).

2.4. Nomagram and Calibration

Considering clinicopathological factors and risk score, a predictive nomogram which was designed to predict 1-, 3-, and 5-year OS was created utilizing R packages "survival", "regplot" and "rms". In the meantime, calibration curves for one-year, three-year, and five-year survival projections were generated to assess the predictive accuracy of the nomogram.

2.5. Gene set enrichment analysis

The Gene Ontology repository categorizes genetic functions into three distinct classi-fications: biological process (BP), cellular component (CC), and molecular function (MF). Utilizing the "clusterProfiler" R computational package, we performed Gene Ontology and Kyoto Encyclopedia of Genes and Genomes (KEGG) pathway enrichment analyses to elu-cidate potentially enriched functional categories and signaling cascades, with subsequent visualization implemented through "GOplot" and "ggplot2" R visualization libraries.

2.6. Investigation of TME, immune infiltration and immune checkpoints

Based on the result of GO and KEGG, we conducted immune-related analyses. ES-TIMATE algorithm is usually utilized to figure out immune, stromal, and comprehensive scores of TME[16]. The ESTIMATE algorithm was implemented through 'limma' and 'ggpubr' R packages to investigate potential associations between risk stratification scores and tumor microenvironment characteristics. Differential infiltration patterns of specific immune cellular subsets between elevated and reduced disulfidptosis score groups un-derwent examination via seven distinct analytical platforms: XCELL, TIMER, QUAN-TISEQ, MCPCOUNTER, EPIC, CIBERSORT, and CIBERSORT-ABS, with results depicted through bubble plot visualization. Multiple R packages including "limma", "scales", "ggplot2", "ggtext", "reshape2", "tidyverse", and "ggpubr" facilitated this analytical process. Subsequently, quantitative assessment of 29 immune cell populations and functional pa-rameters across 448 gastric adenocarcinoma specimens was performed utilizing sin-gle-sample gene set enrichment methodology (ssGSEA) through "GSVA", "limma", and "GSEABase" R packages, with resultant data visualized via dual boxplot representations using "limma", "ggpubr", and "reshape2" software packages. Finally, we conducted im-mune checkpoint analysis to explore differentially expressed immune checkpoints be-tween high and low disulfidptosis score group.

2.7. TMB, MSI and TIDE

Initially, simple nucleotide variation profiles from 434 gastric adenocarcinoma pa-tients were acquired from TCGA repository, with subsequent tumor mutational burden quantification executed through Strawberry Perl computational platform. Mutational landscape visualization via waterfall diagrams depicting the 15 most frequently altered genes in elevated versus reduced risk cohorts was generated using the "maftools" package. Survival analysis curves stratifying patients into four distinct categories ("elevated TMB with high risk", "elevated TMB with low risk", "reduced TMB with high risk", and "re-duced TMB with low risk") were constructed utilizing "survival" and "survminer" R li-braries. Additionally, based on extracted gastric adenocarcinoma microsatellite stability data, graphical representations including bar and box plots were developed to elucidate associations between microsatellite instability status and risk classification scores. Ulti-mately, comparative analysis of Tumor Immune Dysfunction and Exclusion metrics be-tween patient populations with differential disulfidptosis score classifications was per-formed.

2.8. Drug sensitivity analysis

Inhibitory concentration-50 (IC50) measurements for diverse therapeutic agents were determined and juxtaposed between elevated and reduced disulfidptosis score patient cohorts through implementation of the "pRRophetic" R computational package, with re-sultant comparative analyses displayed as boxplots representations.

3. Results

3.1. Data source and processing

Using Strawberry Perl software, we processed the TCGA transcriptome data and gained the expression data of 19938 mRNAs and 16876 lncRNAs. By combining the mRNAs expression profile with 24 disulfidptosis-related genes, we obtained the expres-sion data of 24 DRGs. Then, based on the criteria of |Pearson R|>0.4 and $p < 0.001$, Pear-son correlation analysis between 16876 lncRNAs and 24 DRGs was conducted and 367 drlncRNAs were finally identified (Figure 2A).

3.2. Development and verification of the drlncRNA predictive algorithm

By combining 367 drlncRNAs expression data with 407 GC patients' clinical infor-mation, we acquired the drlncRNAs expression data profile and survival data for 407 samples, which was used for risk model building. We first implemented univariate cox regression analysis and preliminary screening out

29 drlncRNAs (Figure 2B, p<0.05). Subsequently, LASSO-penalized Cox analysis was implemented to mitigate model over-fitting concerns and 7 drlncRNAs significantly related to overall survival (OS) were ob-tained (Figure 2C, D, p<0.05). Eventually, the drlncRNA risk signature comprising 3 lncRNAs (AC107021.2, AC016394.2 and AC129507.1) and corresponding risk coefficient was acquired (Figure 2E, p<0.05). In the meantime, the relationship between 24 DRGs and 3 drlncRNAs is presented in Figure 2F. According to the previous calculation formula, risk score = AC107021.2exp × 0.66000986856416 + AC016394.2exp × -0.435804339506525 + AC129507.1exp × 0.636605050383588.

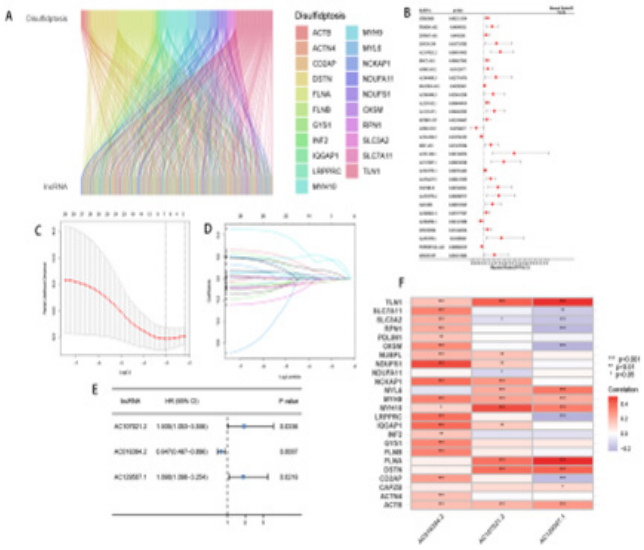

Figure 2. Characterization of drlncRNAs in gastric carcinoma and establishment of a risk signature. (A) Identification of 367 disulfidptosis-related long non-coding RNA tran-scripts within gastric adenocarcinoma specimens. (B) Forest plot visualization represent-ing univariate Cox proportional hazards regression outcomes. (C, D) Application of LASSO regression to the 30 overall survival-associated transcripts determined through univariate Cox regression methodology. (E) Prognostic signature predicated upon disul-fidptosis-related elements was established through multivariable Cox regression analytic approaches. (F) Associative patterns between the prognostic model and disulfidpto-sis-related gene.

A total of 407 STAD samples were then allocated into two groups randomly at a 1:1 ratio. The dataset distribution consisted of 204 specimens allocated to the training cohort and 203 cases assigned to the validation group. Based on the median risk score as cutoff value, patients were divided into high and low risk group. According to the risk score and survival status of train set patients manifested in Figure 3A, B, we can conclude that the mortality of patients was positively correlated with risk score. Obviously, the risk heatmap of 3 drlncRNAs constructed the model (Figure 3C) showed that the upregulated AC107021.2 and AC129507.1 were significantly associated with higher disulfidptosis score, while AC016394.2 was upregulated in the low disulfidptosis score patients. The Kaplan–Meier curve of train set (Figure 3D, p<0.001) indicated that the survival time of patients in the high- risk group were notably lower than that in the low- risk group, which was consistent with our expectations. To demonstrate the predictability of the drlncRNA model, we conducted the same analysis in the test set and whole set. Findings derived from both the validation cohort (Figure 3E-H) and the aggregate patient population (Figure 3I-L) demonstrated concordance with results observed in TCGA training dataset.

Independent prognostic evaluation demonstrated that the 3 drlncRNAs signature constituted a robust survival prediction tool, functioning autonomously from demo-graphic and clinical parameters including patient age and disease stage (Figure 3M, N). Subsequently, ROC curve analysis yielded area under curve measurements within the training population (1-year AUC = 0.741, 3-year AUC = 0.654, and 5-year AUC = 0.781; Figure 3O), validation population (1-year AUC = 0.638, 3-year AUC = 0.640, and 5-year AUC = 0.707; Figure 3P), and comprehensive cohort (1-year AUC = 0.692, 3-year AUC = 0.646, and 5-year AUC = 0.723; Figure 3Q). Area under curve values for receiver operating characteristic analyses across various clinicopathological features were additionally cal-culated, and the ROC curve predicated upon our risk model showed the greatest AUC value (Figure 3R), which illustrated that our risk model as a prognosis predictor was con-siderably accurate.

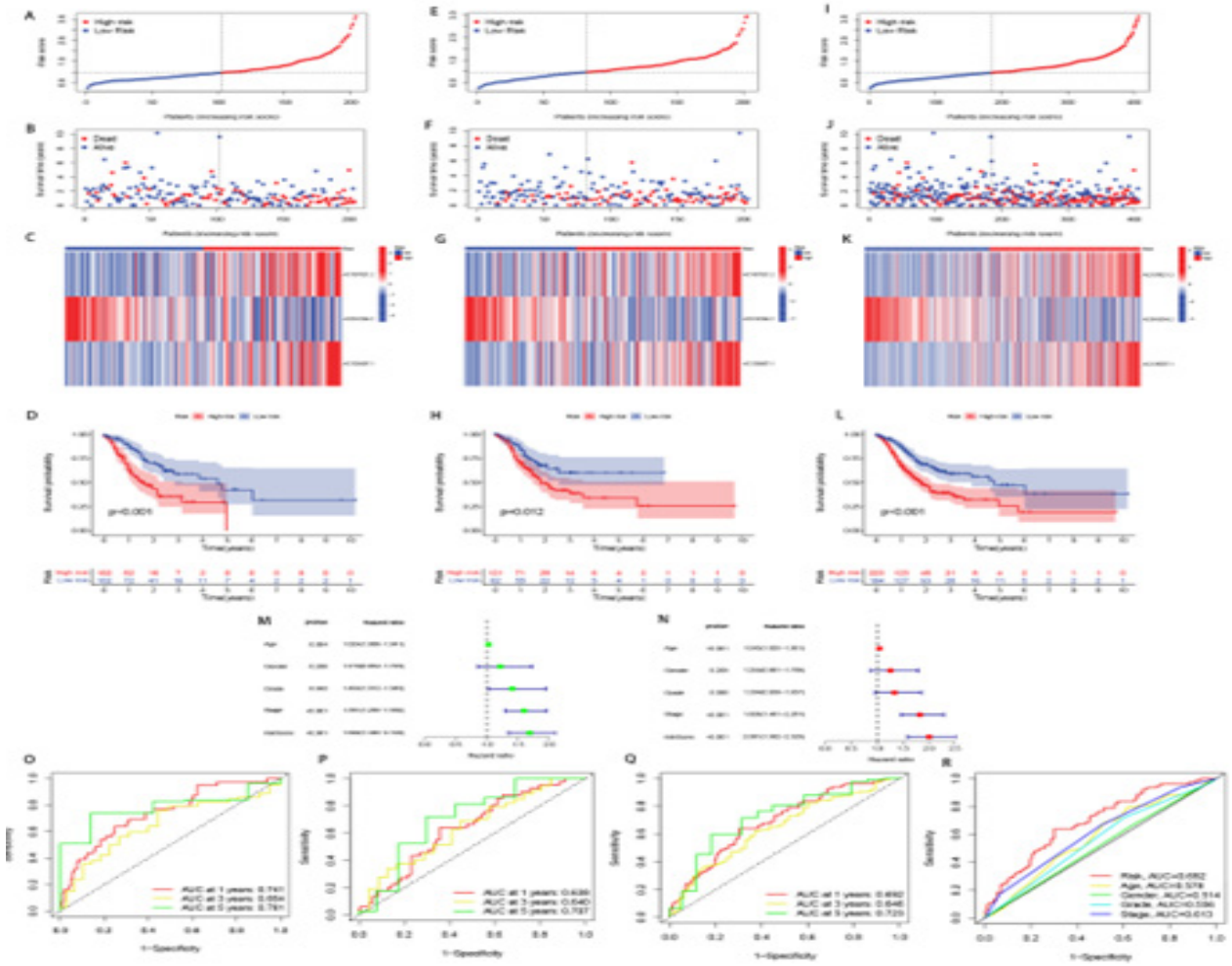

Figure 3. Prognostic assessment of risk stratification algorithm across training, vali-dation, and comprehensive cohorts. (A-D) Comparative analysis of risk distribution, sur-vival outcomes, expression profiles, and prognostic differences between elevated and re-duced disulfidptosis score categories within the training dataset. (E-H, I-L) Parallel ana-lytical evaluation conducted in validation cohort and aggregate patient population. (M) Forest plot visualization depicting univariate Cox proportional hazards regression of di-verse clinicopathological variables. (N) Multivariable Cox regression modeling results. (O-Q) ROC curves representing 1-year, 3-year, and 5-year predictive performance in training dataset, validation cohort, and comprehensive patient population. (R) ROC curves comparing drlncRNA models with different clinical features.

To further substantiate the predictive reliability of our algorithm, Kaplan-Meier sur-vival analyses were generated comparing patient outcomes between elevated and reduced risk classifications across various clinicopathological parameters including patient age, histological differentiation grade, disease progression stage, primary tumor extent (T clas-sification), nodal involvement status (N classification), and metastatic disease presence (M classification). We can recognize that our prognostic signature can accurately prognos-ticate the survival of patients independent of clinical variables (Figure 4). For patients in M1 stage, there was no significant difference in survival between our high and low risk groups, which may be due to the lack of sufficient samples.

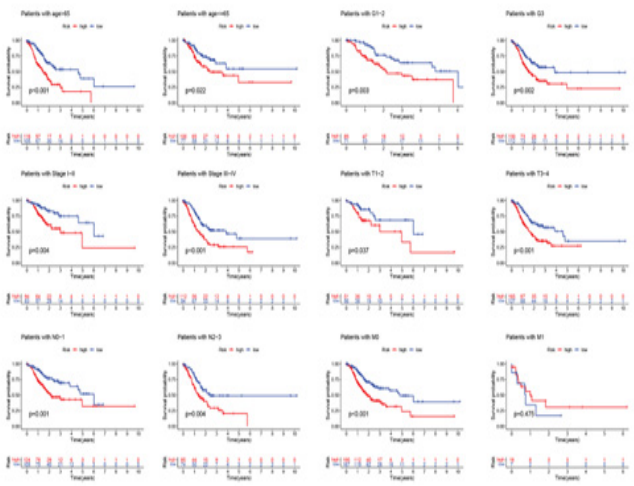

Figure 4. Kaplan-Meier survial analysis for different clinicopathological characteris-tics

3.3. Nomogram and calibration curves

To facilitate survival duration estimation utilizing our disulfidptosis-associated long non-coding RNA profile, we constructed a nomographic prediction model capable of projecting one-year, three-year, and five-year survival probabilities (Figure 5A). Concur-rently, calibration plot analyses were developed to validate the predictive precision of this nomographic representation (Figure 5B).

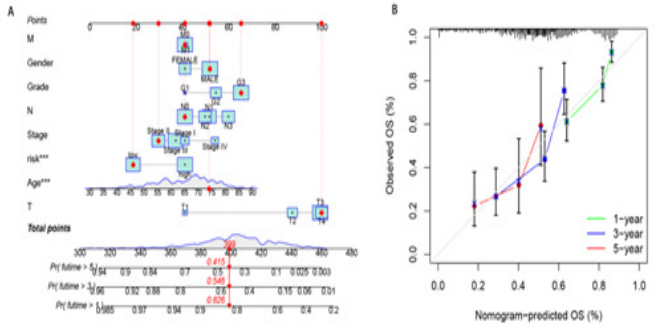

Figure 5. Nomogram development and validation. (A) Integrated prognostic nomo-gram incorporating clinicopathological parameters and disulfidptosis risk classification for overall survival prediction in gastric adenocarcinoma patients (** $p < 0.01$; *** $p < 0.001$). (B) Calibration plot assessment of nomogram accuracy.

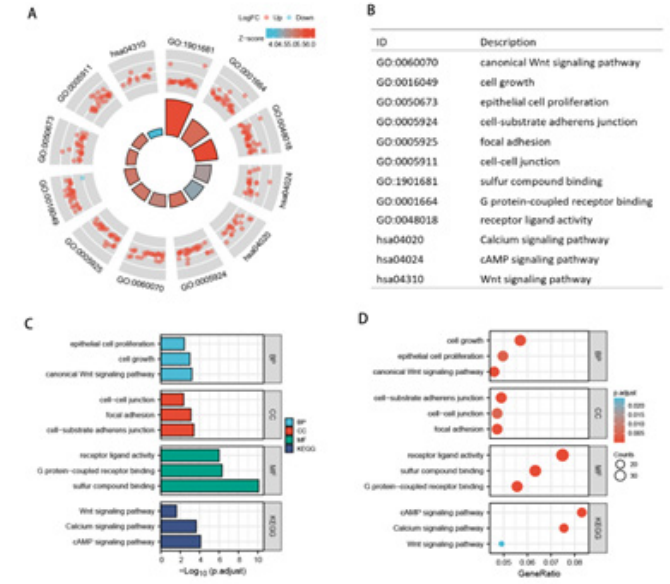

Figure 6. Functional pathway characterization between differential risk stratification cohorts. (A, B) GO enrichment analysis. (C, D) GO and KEGG enrichment analysis.

3.5. Immune infiltration status

For the purpose of exploring the difference of tumor microenvironment between two disulfidptosis score groups, we implemented the Estimation of STromal and Immune cells in MAlignant Tumor tissues using Expression data (ESTIMATE) computational ap-proach to quantify neoplastic tissue purity. According to the boxplots, quantitative as-sessment revealed that elevated risk cohorts exhibited superior scoring metrics compared to their reduced risk counterparts in StromalScore(p=2.5e-10), ImmuneScore(p=0.039) and ESTIMATEScore(p=6.1e-06) (Figure 7A). Subsequently, we analyzed the differences in immune cell subpopulations in TME between two risk groups. The bubble plot visualiza-tion demonstrated that patient cohorts with elevated risk scores corresponded to en-hanced immune cell infiltration density, such as CAF (Cancer associated fibroblast) in XCELL, MCPCOUNTER and EPIC, Macrophage 2 in QUANTISEQ, CIBERSORT and CIBERSORT-ABS (Figure 7B). Additionally, boxplot analyses comparing 29 immune cel-lular populations and functional parameters between risk-stratified cohorts indicated that patients with elevated risk classification exhibited increased MAST cells infiltration cou-pled with diminished MHC class I expression levels (Figure 7C, D). Immune checkpoint molecule evaluation demonstrated upregulated expression patterns of several checkpoints including PDCD-1, CD274 (PD-L1) and CTLA-4 within the reduced risk population (Fig-ure 7E).

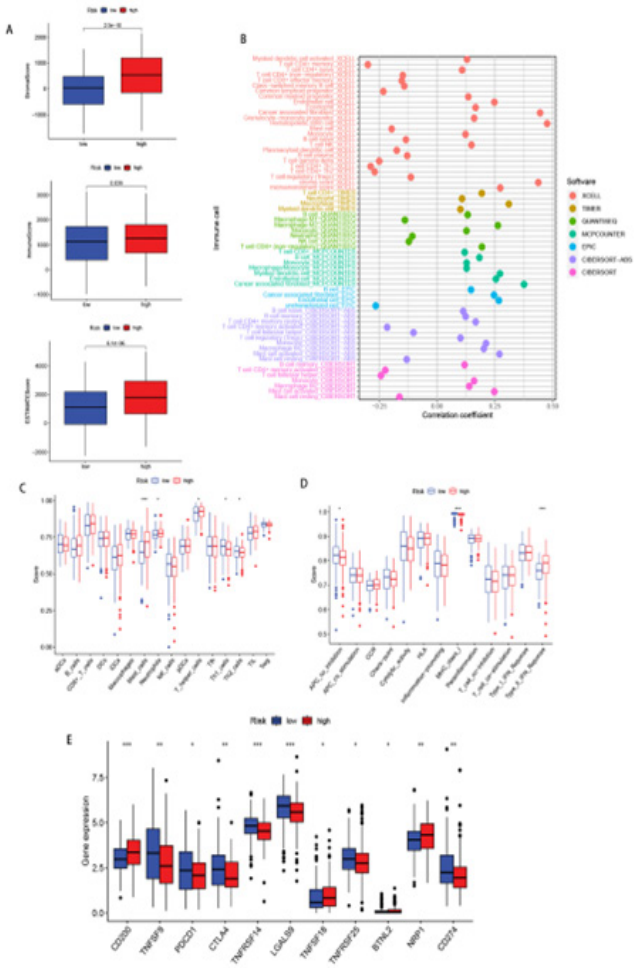

Figure 7. Immunological microenvironment evaluation in gastric adenocarcinoma patients. (A) Comparative assessment of immune infiltration metrics, stromal component quantification, and comprehensive microenvironment estimation between elevated and reduced risk stratification cohorts. (B) Bubble plot visualization depicting immunological cellular composition across risk-stratified populations utilizing seven distinct computa-tional algorithms. (C, D) Boxplots representation of differential immune cell populations and immunological functional parameters between patient cohorts with contrasting risk classifications. (E) Boxplot of expressional variation of ICPs between differential risk cate-gories.

3.6. Immunotherapy response analysis

In this part, TMB, MSI, TIDE analyses were conducted. TMB comparative analysis demonstrated elevated genomic alteration frequencies among patients classified in the reduced risk category (Figure 8A). To comprehensively investigate genetic mutational landscape disparities between risk-stratified cohorts, we generated corresponding muta-tional waterfall visualizations. Within the 15 most frequently mutated genes, exclusively the TP53 tumor suppressor gene exhibited increased mutational prevalence in the high disulfidptosis score patients, and we noticed that the mutation rate of ARID1A gene in the high-risk cohort exhibited substantially diminished prevalence compared to patients clas-sified in the reduced risk population (Figure 8B). Next, we explored the relationship be-tween TMB, patient survival, and risk score (Figure 8C). Survival analysis revealed supe-rior outcomes among gastric carcinoma patients exhibiting elevated tumor mutational burden compared to those with reduced genomic alteration frequencies (p=0.009), with mutational burden status demonstrating independent prognostic significance irrespective of risk stratification metrics. In addition, when we explored the relationship between MSI and risk score, we found that the proportion of patients with “MSI-H” in the low disul-fidptosis score group (32%) was much higher than that in the high disulfidptosis score group (9%) (Figure 8D). The risk score of patients with “MSI-H” was much lower than pa-tients with “MSS” (p=4.7e-10) and “MSI-L” (p=1.7e-05) (Figure 8E). Finally, Tumor Im-mune Dysfunction and Exclusion computational analysis demonstrated elevated im-mune evasion scores among high disulfidptosis cohort (Figure 8F).

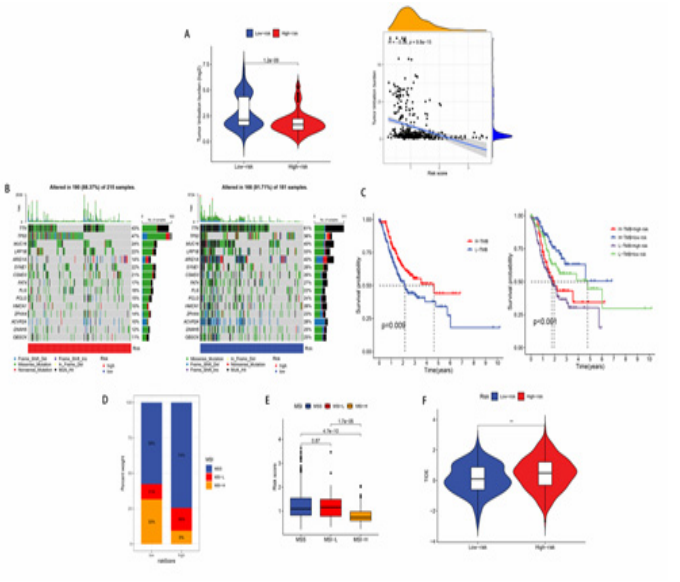

Figure 8. TMB, MSI and TIDE analysis. (A, B) Differential somatic mutational land-scape characterization between elevated and reduced risk patient cohorts. (C) Kaplan-Meier survival analyses across stratified gastric adenocarcinoma patient subpop-ulations. (D, E) Association patterns between risk classification metrics and MSI status. (F) Comparative analysis of TIDE algorithmic scores between contrasting risk stratification categories.

3.7. Drug sensitive analysis

By performing drug sensitivity analysis, we identified a series of drugs (e.g., gemcita-bine, ABT.888) that exhibited lower IC50 values in GC patients with low disulfidptosis scores (Figure 9).

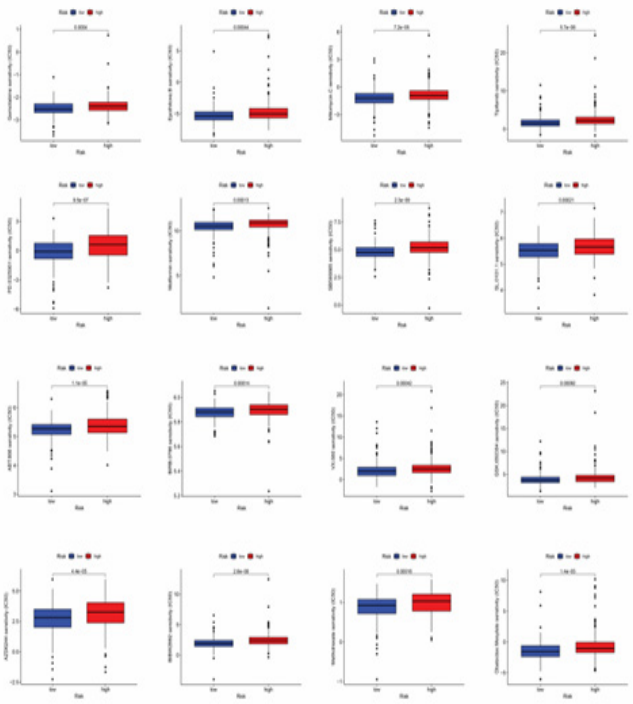

Figure 9. 16 therapeutic agents demonstrating enhanced efficacy in low disulfidpto-sis scores group.

4. Discussion

A literature search revealed 24 genes involved in the disulfidptosis pathway. Co-expression analysis enabled us to identify lncRNAs associated with disulfidptosis. Subsequently, using Cox proportional hazards regression methodology combined with LASSO penalty analysis, we constructed a prognostic signature comprising three disul-fidptosis-associated lncRNAs. AC107021.2 has emerged as a diagnostic marker for gastric and lung adenocarcinomas[17,18], while AC016394.2 and AC129507.1 show diagnostic potential in both gastric adenocarcinoma and prostate carcinoma[19,20]. Nevertheless, the interrelationship between disulfidptosis-associated long non-coding RNA molecules and immunological microenvironment characteristics in gastric adenocarcinoma, along with their prognostic significance, remains to be elucidated. Our study investigated drlncRNAs in gastric cancer and established a three-drlncRNA prognostic signature to predict the prognosis and provide precise and individual clinical treatment guidance for patients with GC.

Through independent prognostic analysis, we demonstrated that our risk model's ability to predict patient outcomes remains significant when accounting for other clinical parameters. ROC curve analyses yielded area under curve measurements, thereby con-firming our risk stratification algorithm's prognostic precision for patient mortality pre-diction across one-year, three-year, and five-year timeframes. Kaplan-Meier curves of dif-ferent clinicopathological parameters including patient age, histological differentiation, disease progression stage, primary tumor dimensions, regional lymphatic involvement, and remote metastatic status, illustrated that our risk model can predict patient outcomes regardless of clinical variables. Through nomogram and calibration curves, our model enables individualized prediction of patient survival at one-year, three-year, and five-year timepoints.

As anticipated, enrichment analysis revealed a strong association between disul-fidptosis-related lncRNAs and sulfur compound binding. The identification of disul-fidptosis revealed a promising therapeutic strategy for cancer treatment, wherein sulfur compound binding orchestrates this cell death process through the activation of specific signaling cascades[10]. GO and KEGG analysis also revealed other functions and pathways that are closely related to drlncRNA, such as GPCR (G protein coupled receptor) binding, cAMP signaling pathway. A recent study revealed that activation of the Gαs-PKA signaling pathway drives CD8+ T cell dysfunction and confers resistance to immuno-therapy[21]. cAMP exhibits dual regulatory effects on tumor cell survival and proliferation through its functional interplay with diverse immunological constituents within TME, particularly T cells and tumor-associated macrophages (TAMs) [22-27].

Given that GO and KEGG enrichment analyses revealed associations between drlncRNAs and immune function, we proceeded to investigate the immune landscape by comparing differential patterns of immunological cellular infiltration between patient co-horts stratified by contrasting risk classifications. The elevated TME scores observed in high-risk patients indicate enhanced immune cell infiltration and enriched stromal cell content in their tumor microenvironment. Macrophages exhibit two distinct polarization states: M1 and M2[28]. In our analysis of immune cell infiltration patterns within the TME, we observed contrasting infiltration levels between M1 and M2 across the two disul-fidptosis score groups: high levels of M1 infiltration were observed in the low-risk group, while high levels of M2 infiltration were observed in the high-risk group. While M1 con-tributes significantly to anti-tumor immunity, M2 facilitate tumor progression by promot-ing immune escape, angiogenesis, and extracellular matrix remodeling in tumor cells[29,30]. This observation potentially elucidates the poor survival of individuals in the high disulfidptosis score group. Besides, the distinctions in sixteen immune cells and thirteen immune-related pathways across two disulfidptosis score groups were investi-gated using ssGSEA (single-sample Gene Set Enrichment Analysis). In the high disul-fidptosis score group, we observed elevated levels of mast cells accompanied by downregulation of MHC class I (Major Histocompatibility Complex I) molecules. A recent study shows that mast cells contribute to resistance against anti-PD-1 immunotherapy, and tar-geted depletion of mast cells enhances the therapeutic efficacy of ICP blockade[31]. Addi-tional research shows that cancer cells can escape immune detection by reducing the ex-pression of MHC-I. This decrease in MHC-I expression represents a key pathway for both inherent and adaptive resistance to immunotherapeutic interventions in cancer pa-tients[32]. Unlike traditional therapy, this approach doesn't directly target tumor cells. In-stead, it works by alleviating immunosuppression and stimulating the body's natural an-ti-tumor immune response, demonstrating remarkable efficacy across various treat-ment-resistant tumors. When combined with chemotherapy, targeted therapy, radiotherapy, and other treatment modalities, it enhances overall therapeutic outcomes[33-36]. El-evated expressional profiles of ICP molecules, including PDCD1, PD-L1, and CTLA-4, in the low disulfidptosis group suggests a potentially enhanced clinical efficacy following immunotherapy.

TMB quantifies the cumulative frequency of nonsynonymous

somatic alterations de-tectable throughout the neoplastic genomic landscape. As molecular prognostic indicator for ICI therapy response, MSI-H demonstrates predictive value across diverse tumor types, potentially due to its role as a mechanistic mediator of immunotherapy outcomes[37]. Accumulating evidence suggests that TMB levels serve as a predictor of patient respon-siveness to immune checkpoint inhibitors, particularly when combined with PD-1 ex-pression and MSI status for enhanced prognostic accuracy[38-41]. Our analysis demon-strated that patients with low disulfidptosis scores exhibited significantly higher tumor mutational burden (TMB) (p=1.2e-09) and a greater proportion of MSI-H cases (32%) compared to the high-score group. Collective observations indicate that patients with low disulfidptosis scores may achieve enhanced therapeutic responses to immunotherapy. Moreover, we found patients with elevated TMB showed improved survival outcomes re-gardless of disulfidptosis scores. To systematically characterize genomic alteration pat-tern disparities between contrasting risk stratification cohorts, we constructed mutational waterfall visualizations representing the fifteen genes exhibiting highest frequency modi-fications. Notably, among the 15 most frequently mutated genes, only the tumor suppres-sor gene TP53 showed a higher mutation frequency in the high-risk group compared to the low-risk group. In contrast, we observed that ARID1A mutations were markedly less prevalent in patients with high disulfidptosis scores, establishing a distinct mutational pattern between two risk classifications. TP53 represents the most frequently mutated gene across human cancers[42]. Its mutations not only compromise its tumor-suppressive functions but also confer oncogenic properties to the mutant p53 protein[43]. Studies have demonstrated that TP53 mutations correlate with poor clinical outcomes in cancer pa-tients[44]. This observation, on the other hand, provides a mechanistic explanation for the poor survival outcomes observed in patients with high disulfidptosis scores. Multiple clinical trials have demonstrated that ARID1A-mutated solid tumors exhibit enhanced responsiveness to immune checkpoint inhibitor interventions across diverse malignancy classifications, independent of MSI status or TMB[45-47]. Collective observations indicate that individuals with high disulfidptosis scores may exhibit resistance to immune check-point inhibitor therapy.

TIDE analysis further showed that patients with high disulfidptosis scores exhibited an increased probability of developing resistance to immunotherapy, suggesting limited therapeutic benefit from immune checkpoint blockade in this subgroup. Moreover, com-prehensive drug sensitivity analysis identified multiple potential therapeutic agents that showed enhanced efficacy in reduced-risk classification, while also revealing drugs prone to resistance in the increased-risk classification, thereby providing valuable insights for personalized treatment strategies. Contemporary clinical investigations have established that the combination of gemcitabine plus cisplatin with PD-L1 inhibitors exhibits prom-ising therapeutic efficacy in patients with advanced biliary tract cancer[48]. In another phase I dose-escalation study, the combination of ABT.888(veliparib) with PD-1 inhibitor plus platinum-based doublet chemotherapy demonstrated promising therapeutic efficacy in patients with metastatic or advanced non-small cell lung cancer[49]. According to these results, the combination of ICIs with conventional chemotherapeutic agents represents a promising therapeutic strategy for gastric cancer.

Additionally, we realized that this study still had limitations. Firstly, the 3 drlncRNAs prognostic model was developed and verified in light of the findings from retrospective analyses of TCGA. It is necessary to conduct prospective cohort studies to further validate this risk model. Secondly, more independent immunotherapy cohorts were needed to confirm the predictive value of the prognostic signature for immunother-apy response. Lastly, validation of this predictive framework's reliability and clinical im-plementation value necessitates acquisition of extensive patient datasets, complemented by mechanistic investigations into how these long non-coding RNA molecules influence gastric carcinoma initiation and progression.

5. Conclusions

In summation, our established disulfidptosis-related lncRNA prognostic model ena-bles accurate prediction of patient survival and facilitates the identification of potentially effective drugs and treatment-sensitive individuals, ultimately contributing to improved survival outcomes in STAD patients.

References

1. Van Cutsem E, Sagaert X, Topal B, Haustermans K, Prenen H (2016) Gastric cancer. Lancet (London, England), 388: 2654-2664. doi:10.1016/s0140-6736(16)30354-3.

2. Morga, E, Arnold M, Camargo MC, Gini A, Kunzmann AT, et al. (2022). The current and future incidence and mortality of gastric cancer in 185 countries, 2020–40: a population-based modelling study. EClinicalMedicine, 47. 101404, doi:10.1016/j.eclinm.2022.101404.

3. Thrift AP, El-Serag HB (2020) Burden of gastric cancer. Clinical gastroenterology and hepatology 18: 534-542. doi:10.1016/j.cgh.2019.07.045.

4. Karimi P, Islami F, Anandasabapathy S, Freedman ND, Kamangar F (2014) Gastric cancer: descriptive epidemiology, risk factors, screening, and prevention. Cancer epidemiology, biomarkers & prevention 23: 700-713. doi:10.1158/1055-9965.Epi-13-1057.

5. Liu X, Meltzer SJ (2017) Gastric cancer in the era of precision

medicine. Cellular and molecular gastroenterology and hepatology 3: 348-358. doi:10.1016/j.jcmgh.2017.02.003.

6. Jin X, Liu Z, Yang D, Yin K, Chang X (2022) Recent progress and future perspectives of immunotherapy in advanced gastric cancer. Frontiers in immunology 13: 948647. doi:10.3389/fimmu.2022.948647.

7. Vareki SM, Garrigós C, Duran I (2017) Biomarkers of response to PD-1/PD-L1 inhibition. Critical reviews in oncology/hematology 116: 116-124. doi:10.1016/j.critrevonc.2017.06.001.

8. Liu X, Nie L, Zhang Y, Yan Y, Wang C, et al. (2023). Actin cytoskeleton vulnerability to disulfide stress mediates disulfidptosis. Nature cell biology, 25(3), 404-414. doi:10.1038/s41556-023-01091-2.

9. Koppula P, Zhuang L, Gan B (2021) Cystine transporter SLC7A11/xCT in cancer: ferroptosis, nutrient dependency, and cancer therapy. Protein & cell 12: 599-620. doi:10.1007/s13238-020-00789-5.

10. Zheng T, Liu Q, Xing F, Zeng C, Wang W (2023) Disulfidptosis: a new form of programmed cell death. Journal of Experimental & Clinical Cancer Research 42: 137. doi:10.1186/s13046-023-02712-2.

11. Zheng P, Zhou C, Ding Y, Duan S (2023) Disulfidptosis: a new target for metabolic cancer therapy. Journal of Experimental & Clinical Cancer Research 42:103. doi:10.1186/s13046-023-02675-4.

12. Shuai Y, Ma Z, Liu W, Yu T, Yan C, et al. (2020). TEAD4 modulated LncRNA MNX1-AS1 contributes to gastric cancer progression partly through suppressing BTG2 and activating BCL2. Molecular cancer 19: 1-20. doi:10.1186/s12943-019-1104-1.

13. Sun D, Gou H, Wang D, Li C, Li Y, et al. (2022). LncRNA TNFRSF10A-AS1 promotes gastric cancer by directly binding to oncogenic MPZL1 and is associated with patient outcome. International Journal of Biological Sciences 18: 3156. doi:10.7150/ijbs.68776.

14. Qi F, Liu X, Wu H, Yu X, Wei C, et al. (2017). Long noncoding AGAP2-AS1 is activated by SP1 and promotes cell proliferation and invasion in gastric cancer. Journal of Hematology & Oncology 10: 1-14. doi:10.1186/s13045-017-0420-4.

15. Liu YW, Xia R, Lu K, Xie M, Yang F, et al. (2017). LincRNA FEZF1-AS1 represses p21 expression to promote gastric cancer proliferation through LSD1-mediated H3K4me2 demethylation. Molecular cancer 16: 1-16. doi:10.1186/s12943-017-0588-9.

16. Mao M, Yu Q, Huang R, Lu Y, Wang Z, et al. (2020). Stromal score as a prognostic factor in primary gastric cancer and close association with tumor immune microenvironment. Cancer Medicine 9: 4980-4990. doi:10.1002/cam4.2801.

17. Fan Z, Wang Y, Niu R (2022) Identification of the three subtypes and the prognostic characteristics of stomach adenocarcinoma: Analysis of the hypoxia-related long non-coding RNAs. Functional & Integrative Genomics 22: 919-936. doi:10.1007/s10142-022-00867-3.

18. Mao F, Li Z, Li Y, Huang H, Shi Z, et al. (2022). Necroptosis-related lncRNA in lung adenocarcinoma: a comprehensive analysis based on a prognosis model and a competing endogenous RNA network. Frontiers in genetics 13: 940167. doi:10.3389/fgene.2022.940167.

19. Lu Y, Wu J, Li X, Leng Q, Tan J, et al. (2024). Cuproptosis-related lncRNAs emerge as a novel signature for predicting prognosis in prostate carcinoma and functional experimental validation. Frontiers in immunology 15: 1471198. doi:10.3389/fimmu.2024.1471198.

20. Kang K, Li X, Peng Y, Zhou Y (2023) Comprehensive analysis of disulfidptosis-related lncrnas in molecular classification, immune microenvironment characterization and prognosis of gastric cancer. Biomedicines 11: 3165. doi:10.3390/biomedicines11123165.

21. Wu VH, Yung BS, Faraji F, Saddawi-Konefka R, Wang Z, et al. (2023). The GPCR–Gαs–PKA signaling axis promotes T cell dysfunction and cancer immunotherapy failure. Nature immunology 24: 1318-1330. doi:10.1038/s41590-023-01529-7.

22. Wu JJ, Yang Y, Peng WT, Sun JC, Sun WY, et al. (2019). G protein-coupled receptor kinase 2 regulating β2-adrenergic receptor signaling in M2-polarized macrophages contributes to hepatocellular carcinoma progression. OncoTargets and therapy 5499-5513. doi:10.2147/ott.S209291.

23. Yano S, Ghosh P, Kusaba H, Buchholz M, Longo DL (2003) Effect of promoter methylation on the regulation of IFN-γ gene during in vitro differentiation of human peripheral blood T cells into a Th2 population. The Journal of Immunology 171: 2510-2516. doi:10.4049/jimmunol.171.5.2510.

24. Qian X, Gu L, Ning H, Zhang Y, Hsueh EC, et al. (2013). Increased Th17 cells in the tumor microenvironment is mediated by IL-23 via tumor-secreted prostaglandin E2. The Journal of Immunology 190: 5894-5902. doi:10.4049/jimmunol.1203141.

25. Ji Y, Zhang W (2010) Th17 cells: positive or negative role in tumor? Cancer Immunology, Immunotherapy 59: 979-987. doi:10.1007/s00262-010-0849-6.

26. Asadzadeh Z, Mohammadi H, Safarzadeh E, Hemmatzadeh M, Mahdian-Shakib A, et al. (2017). The paradox of Th17 cell functions in tumor immunity. Cellular immunology 322: 15-25. doi:10.1016/j.cellimm.2017.10.015.

27. Zhang H, Liu Y, Liu J, Chen J, Wang J, et al. (2024). cAMP-PKA/EPAC signaling and cancer: the interplay in tumor microenvironment. Journal of Hematology & Oncology 17: 5. doi:10.1186/s13045-024-01524-x.

28. Huang YC, Feng ZP (2013) The good and bad of microglia/macrophages: new hope in stroke therapeutics. Acta Pharmacologica Sinica 34: 6-7. doi:10.1038/aps.2012.178.

29. Aras S, Zaidi MR (2017) TAMeless traitors: macrophages in cancer progression and metastasis. British journal of

cancer 117: 1583-1591. doi:10.1038/bjc.2017.356.

30. Toledo B, Zhu Chen L, Paniagua-Sancho M, Marchal JA, Perán M, et al. (2024). Deciphering the performance of macrophages in tumour microenvironment: a call for precision immunotherapy. Journal of hematology & oncology 17: 44. doi:10.1186/s13045-024-01559-0.

31. Somasundaram R, Connelly T, Choi R, Choi H, Samarkina A, et al. (2021). Tumor-infiltrating mast cells are associated with resistance to anti-PD-1 therapy. Nature communications 12: 346. doi:10.1038/s41467-020-20600-7.

32. Taylor BC, Balko JM (2022) Mechanisms of MHC-I downregulation and role in immunotherapy response. Frontiers in immunology 13: 844866. doi:10.3389/fimmu.2022.844866.

33. Janjigian YY, Shitara K, Moehler M, Garrido M, Salman P, et al. (2021). First-line nivolumab plus chemotherapy versus chemotherapy alone for advanced gastric, gastro-oesophageal junction, and oesophageal adenocarcinoma (CheckMate 649): a randomised, open-label, phase 3 trial. The Lancet 398: 27-40. doi:10.1016/s0140-6736(21)00797-2.

34. Pennock GK, Chow LQ (2015) The evolving role of immune checkpoint inhibitors in cancer treatment. The oncologist 20: 812-822. doi:10.1634/theoncologist.2014-0422.

35. Ribas A,Wolchok JD (2018) Cancer immunotherapy using checkpoint blockade. Science 359: 1350-1355. doi:10.1126/science.aar4060.

36. Gaikwad S, Agrawal MY, Kaushik I, Ramachandran S, Srivastava SK (2022). Immune checkpoint proteins: Signaling mechanisms and molecular interactions in cancer immunotherapy. In Seminars in cancer biology 86: 137-150. Academic Press. doi:10.1016/j.semcancer.2022.03.014.

37. Ionov Y, Peinado MA, Malkhosyan S, Shibata D, Perucho M (1993) Ubiquitous somatic mutations in simple repeated sequences reveal a new mechanism for colonic carcinogenesis. Nature 363: 558-561. doi:10.1038/363558a0.

38. Wang X, Lamberti G, Di Federico A, Alessi J, Ferrara R, et al. (2024). Tumor mutational burden for the prediction of PD-(L) 1 blockade efficacy in cancer: challenges and opportunities. Annals of Oncology 35: 508-522. doi:10.1016/j.annonc.2024.03.007.

39. Wang F, Wei XL, Wang FH, Xu N, Shen L, et al. (2019). Safety, efficacy and tumor mutational burden as a biomarker of overall survival benefit in chemo-refractory gastric cancer treated with toripalimab, a PD-1 antibody in phase Ib/II clinical trial NCT02915432. Annals of Oncology 30: 1479-1486. doi:10.1093/annonc/mdz197.

40. 40. Robert C, Lewis KD, Gutzmer R, Stroyakovskiy D, Gogas H, et al. (2022). Biomarkers of treatment benefit with atezolizumab plus vemurafenib plus cobimetinib in BRAFV600 mutation–positive melanoma. Annals of Oncology 33: 544-555. doi:10.1016/j.annonc.2022.01.076.

41. Budczies J, Kazdal D, Menzel M, Beck S, Kluck K, et al. (2024). Tumour mutational burden: clinical utility, challenges and emerging improvements. Nature Reviews Clinical Oncology 21: 725-742. doi:10.1038/s41571-024-00932-9.

42. Kastenhuber ER, Lowe SW (2017) Putting p53 in context. Cell 170: 1062-1078. doi:10.1016/j.cell.2017.08.028.

43. Hu J, Cao J, Topatana W, Juengpanich S, Li S, et al. (2021). Targeting mutant p53 for cancer therapy: direct and indirect strategies. Journal of hematology & oncology 14: 1-19. doi:10.1186/s13045-021-01169-0.

44. Olivier M, Hollstein M, Hainaut P (2010) TP53 mutations in human cancers: origins, consequences, and clinical use. Cold Spring Harbor perspectives in biology 2: a001008. doi:10.1101/cshperspect.a001008.

45. Okamura R, Kato S, Lee S, Jimenez RE, Sicklick JK, et al. (2020). ARID1A alterations function as a biomarker for longer progression-free survival after anti-PD-1/PD-L1 immunotherapy. Journal for immunotherapy of cancer 8: e000438. doi:10.1136/jitc-2019-000438.

46. Goswami S, Chen Y, Anandhan S, Szabo PM, Basu S, et al. (2020). ARID1A mutation plus CXCL13 expression act as combinatorial biomarkers to predict responses to immune checkpoint therapy in mUCC. Science translational medicine 12: eabc4220. doi:10.1126/scitranslmed.abc4220.

47. Li L, Li M, Jiang Z, Wang X (2019) ARID1A mutations are associated with increased immune activity in gastrointestinal cancer. Cells8: 678. doi:10.3390/cells8070678.

48. Hindson J (2022) Gemcitabine and cisplatin plus immunotherapy in advanced biliary tract cancer: a phase II study. Nature Reviews Gastroenterology & Hepatology 19: 280-280. doi:10.1038/s41575-022-00616-8.

49. Clarke JM, Patel JD, Robert F, Kio EA, Thara E, et al. (2021). Veliparib and nivolumab in combination with platinum doublet chemotherapy in patients with metastatic or advanced non-small cell lung cancer: A phase 1 dose escalation study. Lung Cancer 161: 180-188. doi:10.1016/j.lungcan.2021.09.004.